The Application of Fluid Dynamic Gauging in Characterising Cake Deposition during the Cross-Flow Microfiltration of a Yeast Suspension

William J. T. Lewis, Y. M. John Chew*, Michael R. Bird

Department of Chemical Engineering, University of Bath, Claverton Down, Bath, BA2 7AY, UK
** Corresponding author (jc604@bath.ac.uk)*

Abstract

Fluid Dynamic Gauging (FDG) has been used to study cake fouling during cross-flow microfiltration of inactive *Saccharomyces cerevisiae* yeast suspensions through a 5 μm nominal pore size mixed cellulose ester membrane. Cake thickness was measured *in-situ* and in real-time during fouling, for which an initial growth rate of *ca*. 0.81 μm·s^{-1} was observed at TMP = 35 mbar and Re_{duct} = 1000. The thickness increased asymptotically to a terminal value of 130 μm, limited by the FDG process. Although it influences the evolution of the cake thickness, FDG can nevertheless be used to perform strength tests on preformed cakes, by imposing controlled shear stresses to the surface and measuring the thickness following deformation. Cake deformation via incremental increases in shear stress demonstrated that the cake's resilience to tangential fluid shear was inversely proportional to its thickness. It was found that preformed cakes over 250 μm thick were deformed by shear stresses < 10 N·m^{-2}, indicating very loose cohesion between cells on the cake's surface. The range and accuracy of thickness measurements is subject to the strength of fouling layers and the operating conditions of the apparatus. Measures to enhance the technique's efficacy have been identified and are currently underway.

Keywords: Fluid Dynamic Gauging, microfiltration, Fouling, Cleaning, yeast,

Nomenclature:

C_b	Bulk particle concentration (kg·m^{-3})
C_d	Discharge coefficient
C_w	Particle concentration at the membrane surface (kg·m^{-3})
d	Gauging tube diameter (m)
D	Width of duct (m)

d_H	Hydraulic diameter (m)
d_p	Particle diameter (m)
D_p	Particle diffusivity ($m^2 \cdot s^{-1}$)
d_t	Nozzle throat diameter (m)
g	Gravitational constant ($m \cdot s^{-2}$)
h	Nozzle clearance from deposit (m)
h_0	Nozzle clearance from substrate (m)
J	Permeate flux ($m \cdot s^{-1}$)
J'	Relative flux
J_0	Initial flux ($m \cdot s^{-1}$)
k_b	Boltzmann constant ($m^2 \cdot kg \cdot s^{-2} \cdot K^{-1}$)
k_m	Convective diffusion mass transfer coefficient ($m \cdot s^{-1}$)
k_s	Particle settling mass transfer coefficient ($m \cdot s^{-1}$)
k_t	Observed mass transfer coefficient ($m \cdot s^{-1}$)
L	Length of porous section of duct (m)
M	Mass of cake per unit area ($g \cdot m^{-2}$)
m_g	Gauging flowrate ($g \cdot s^{-1}$)
m_p	Permeate flow ($g \cdot s^{-1}$)
Δp_{ij}	Pressure difference between stations i and j (Pa)
Pr	Prandtl number
r	Radial distance from centre of nozzle (m)
Re_{duct}	Reynolds number based on duct width, D
R_m	Membrane resistance (m^{-1})
s	Width of nozzle rim (m)
Sc	Schmidt number
Sh	Sherwood number
t	Time (s)
T	Temperature (K)
TMP	Transmembrane pressure (Pa)
u_t	Terminal velocity of a particle ($m \cdot s^{-1}$)
x_i	Volume fraction of total particles with a diameter i

Greek letters

μ	Fluid viscosity ($kg \cdot m^{-1} \cdot s^{-1}$)
δ	Cake thickness (m)
ε	Cake voidage
ρ	Fluid density ($kg \cdot m^{-3}$)
ρ_p	Particle density ($kg \cdot m^{-3}$)
τ_w	Maximum shear stress on the surface below gauging nozzle ($N \cdot m^{-2}$)

Abbreviations

CFD	Computational Fluid Dynamics
CFMF	Cross-Flow Microfiltration
DOTM	Direct Observation Through the Membrane
DVO	Direct Visual Observation
EPSRC	Engineering and Physical Sciences Research Council
FDG	Fluid Dynamic Gauging
MF	Microfiltration
NIR-NLOI	Near Infrared Nonlinear Optical Imaging
NMR	Nuclear Magnetic Resonance
SEM	Scanning Electron Microscopy
SSE	Sum of Squares due to Error
UTDR	Ultrasonic Time Domain Reflectometry

1. Introduction

Membrane separations offer numerous advantages over conventional separation techniques. These include greater selectivity, lower energy consumption, and a modular design which allows for predictable scale-up [1]. Microfiltration (MF) membranes are the most commonly used class of membranes industrially, occupying *ca.* 50% of the US membrane market value in 2001, more than twice that of any other category of membrane [2]. Ubiquitous in all applications of membrane technology is the issue of fouling, which can affect the performance and lifespan of the membrane.

Research into the reduction and removal or prevention of fouling has dominated membrane research over the past twenty years, and of particular note are the recent advances in the study of reversible cake fouling. Direct Visual Observation (DVO) [3-5] and Direct Observation Through the Membrane (DOTM) [6-8] techniques have been important in understanding the mechanisms of deposition and removal of particles on MF membrane surfaces; whilst various high-tech methods such as Laser Triangulometry [9-11], Ultrasonic Time Domain Reflectometry (UTDR) [12-14], near infrared nonlinear optical imaging (NIR-NLOI) [15], and Nuclear Magnetic Resonance (NMR) imaging [16] have gone some way towards characterising deposited cake layers. Chen et al. [17] provide a comprehensive review of these and other non-invasive techniques used to study membrane fouling. So far studies of reversible cake fouling have concentrated on initial deposition or progressive thickness. The removal process, with regards to the strength and tenacity of such layers, has received little attention.

In this work we present the application of pressure mode Fluid Dynamic Gauging (FDG) for estimating the thickness and cohesive strength of cake layers in cross-flow microfiltration of inactive yeast suspensions through a 5 μm nominal pore size cellulosic membrane. Although not strictly considered as non-invasive, this technique has proven an effective non-contact method for measuring cake-layer thickness in both dead-end [18], and cross-flow filtrations [19-21]. FDG also allows the study of flow-induced cake removal by combining thickness measurements with controlled application of fluid shear to the surface of the cake. Whilst in previous work FDG was used to study fouling by a monodisperse, inorganic suspension [20], this study focuses on demonstrating how it can be applied to the filtration of a more complex organic suspension which more closely represents those filtered in food processes.

1.1 Fluid Dynamic Gauging (FDG)

Although FDG has become a well-established technique for fouling studies on non-porous surfaces in static [22] and flowing [23] environments, its application to the study of membrane fouling, especially in cross-flow microfiltration (CFMF), is still a relatively new practice. So far FDG studies on CFMF have been performed on monodisperse ballotini suspensions under laminar flow conditions [20], and sugar beet molasses solutions under turbulent conditions[19, 21].

The principle of pressure mode FDG is shown schematically in figure 1. Fluid is drawn through a nozzle at a constant flow rate, m_g; and the differential pressure across the gauge between stations 1 and 4 on figure 1, Δp_{14}, is governed by the clearance, h, of the nozzle from a surface. Flow into the nozzle and its relation to differential pressure can be characterised by a dimensionless discharge coefficient, C_d; defined as the ratio of actual to ideal mass flow through the nozzle:

$$C_d = \frac{m_{g\ (actual)}}{m_{g\ (ideal)}} = \frac{m_g}{\frac{\pi d_t^2}{4}\sqrt{2\rho\Delta p_{13}}} \tag{1}$$

where ρ is the density of the fluid and Δp_{13} is the pressure difference between stations 1 and 3, given by:

$$\Delta p_{13} = \Delta p_{14} - \Delta p_{34} \tag{2}$$

where Δp_{34} can be estimated using the Hagen-Poiseuille solution. A more detailed analysis of this derivation is given in [24].

Assuming that the deposit acts as a flat, relatively non-porous and non-slip surface; the clearance of the nozzle, h, can be estimated from a correlation between C_d and a characteristic height, h/d_t, for a set of known h values. An example of this is shown by the open symbols in figure 2. The thickness of a deposit, δ, in the area directly below the gauge is then given by:

$$\delta = h_0 - h \tag{3}$$

where h_0 is the distance between the nozzle and the substrate, determined independently. An optimum operating region for thickness measurements at $h/d_t \leq 0.25$ was identified by Tuladhar

et al. [24], wherein the resistance to flow is governed by the clearance of the nozzle from a surface rather than the diameter of the throat. This is demonstrated in figure 2 where the relationship between C_d and h/d_t transitions from incremental to asymptotic Corresponding values for Δp_{13} are also shown in this figure, for which a similar pattern in the opposite direction is evident. Only thickness estimates from within the incremental region are considered valid, and the most accurate estimates can be made at clearances where $0.1 \leq h/d_t \leq 0.2$, and C_d increases more substantially with h/d_t. It is worth noting that for a surface which is not perfectly flat it is probable that, due to the nature of this method, a thickness value representing a rough average over the circular cross section directly underneath the nozzle will be attained. Earlier work [18, 19] has shown that the technique works in the same way for porous surfaces as for flat impermeable surfaces.

Coupled with Computational Fluid Dynamics (CFD), FDG can also be used to measure the cohesive and adhesive strength of a deposit [19]. The flow of fluid into the gauge imposes a tangential shear stress, τ_w, upon the surface directly below the rim of the nozzle. The strength of a deposit can be inferred as the maximum shear stress at which deformation (i.e. a decrease in thickness) is observed. Schmitz and Prat [25] have demonstrated, through numerical modelling, that the effect of slip velocity at the membrane surface can be considered negligible to the membrane performance; thus the no slip boundary condition is imposed at the membrane surface [26]. Whilst it can be estimated using CFD simulations, shear stress can also be approximated by an analytical solution for converging radial flow between parallel disks [27]:

$$\tau_w = \mu \left(\frac{3 m_g}{\rho \pi h^2} \right) \frac{1}{r} \tag{4}$$

where r is the radial distance from the centre of the nozzle. Previous researchers have demonstrated good agreement between this model and CFD simulations for both quasi-static [23] and duct flow systems [28]. Figure 3 shows preliminary data from CFD simulations of FDG during a membrane filtration, the methods of which are described elsewhere [25], and comparison with the curve given by equation (4). At a given clearance, h, and constant gauging flow, m_g , shear stress is proportional to $1/r$, with the maximum shear stress, $\tau_{w,\,max}$, imposed on the surface below the nozzle occurring at the lower limit for r in this circumstance, at a radial position $r = d_t/2$. Currently equation (4) is considered to give a more accurate approximation for $\tau_{w,\,max}$ compared with that of preliminary CFD simulations, so it will be applied when measuring cohesive strength of cakes in this work. It is however, only applicable in the area directly below the nozzle rim, i.e. where $d_t/2 \leq r \geq d_t/2+s$.

The use of pressure mode FDG provides a number of advantages over the initial FDG configurations, wherein the differential pressure, Δp_{14} , is set and the gauging flow, m_g , is measured [29]. Controlling the gauging flow allows for more accurate control of shear stress applied to the deposit and enables the user to reduce the rate of fluid withdrawal from the system, preserving bulk-flow conditions. It also opens up the technique to applications at a greater range of internal or trans-membrane pressures with a higher threshold than in previous work (which used hydrostatic pressure), as demonstrated by Jones *et al*. [19, 21].

2. Experimental

2.1 Materials

2.1.1 Pressure mode FDG apparatus

A schematic of the flow loop used in this work is shown in figure 4a. The suspension was circulated in a loop from a 15 L feed tank, through a *Rotameter* (variable area flow meter) and 500 mm long, 15 mm square brass entry section directly before the test section. A differential pressure transducer, dP_1 (*Omega Engineering*, PX26-005DV, ± 1 mbar) was used to measure TMP by connecting it via flexible couplings to pressure tappings on the feed and permeate side of the test section, and linked to a data logging PC. Similarly, a differential pressure transducer, dP_2 (*Omega Engineering*, PX26-001DV, ± 0.25 mbar) was used to measure Δp_{14}, which was connected to pressure tappings into the test section and an X-piece downstream of the gauge. Both pressure transducers have a response time of 1 ms. TMP and flow rate through the test section (which can be characterised by Re_{duct}, based on the width, D, of the duct) were controlled with valves V1 and V2, whilst a needle valve was used to control gauging flow, m_g. Electronic balances (*A&D*, FX-3000i, ± 0.01 g) were used to measure permeate flow rate, m_p, and gauging flow rate, m_g, by linkage to the data logging PC. LabView 2010 (*National Instruments*) was used for data logging and thickness estimations.

A schematic of the test section is shown in figure 4b. Membranes (M) were mounted on top of a stainless steel mesh (S) and secured within two pieces of transparent *Perspex* along with a rubber seal (RS) to prevent leakage. This assembly resulted in a square duct 15 mm wide and 150 mm long. The membrane itself is located at the base of a 3 mm channel along the bottom of the channel. It should be noted that this sudden step down to the membrane was shown in preliminary simulations (not shown in this report) to cause some minor turbulence and recirculation near the entrance of the duct, but laminar conditions were reached before flow approached the gauge. A gauge (G) of dimensions (from figure 1) d = 4 mm, d_t = 1 mm, s = 0.5 mm, and α = 30°was inserted through the top of the test section and a micrometer (Mi)

was used to adjust and measure its clearance from the membrane. Bleed points (BP) were used to evacuate air bubbles from the system.

2.1.2 Membranes

Mixed cellulose ester membranes of 5 μm nominal pore size were obtained from *Millipore inc.* (catalogue number SMWP29325). The membrane resistance, R_m, was characterised from Darcy's law (equation (5)) by measuring membrane flux, J, and trans-membrane pressure, TMP, during dead-end filtration using apparatus described in previous work [18].

$$J = \frac{TMP}{\mu R_m} \tag{5}$$

Experimental results gave a mean resistance of $R_m = 1.17\times10^{10}$ m^{-1}.

2.1.3 Suspension

Dried, inactive *Saccharomyces cerevisiae* yeast obtained from *Sigma-Aldrich* (Catalogue number 51475) was used as the model foulant. This was suspended in RO water (pH 6.1, conductivity 7-10 μS), which was degassed using a vacuum chamber (*Island Scientific*) and pump (*Edwards* E2M2) in order to prevent the development of air bubbles which would interfere with the FDG operation. A low concentration of 1 $g{\cdot}L^{-1}$ yeast powder (0.09 vol%) was used for all experiments detailed in this report so that viscosity and density changes could be considered negligible. Upon addition of the powdered yeast, a pH drop from 6.1 to 5.9 was observed, measured using a handheld probe (*Hanna Instruments*, p-HEP).

The suspension was characterised by light microscope (*Nikon* Diaphon 300) and by a laser diffraction particle sizer (*Coulter* LS230). The latter of these methods used the Mie solution to Maxwell's equations and a diffractive index for yeast of 1.38 (as derived by Malone [30]), the results for which are shown in figure 5. Two distinct peaks were identified from size distributions using laser diffraction, the first of which was for the diameter of single cells, the latter indicating larger aggregates of around 150 μm diameter. Single cells exhibited an average diameter of 5.8 μm (which was also confirmed using a light microscope), and constituted around 40% (by volume) of the particles in suspension. Significant aggregation was also observed, with aggregates as large as 300 μm diameter present. Overall around 50% of suspended material was individual cells and aggregates < 20 μm diameter and a further 25% were also < 100 μm diameter. Particle characterisation suggested the presence of some cell debris and/or other

unknown impurities (10% of particles were < 2.5 μm diameter), and rehydrated yeast suspensions are thought to exhibit "sticky" substances on cell walls [31]. The suspension studied in this work was therefore considered to more closely represent the complex nature of media processed by microfiltration in the food industry. One such example would be the clarification of beer, for which feeds can contain a mixture of cells, aggregates, sugars and macromolecules [32].

2.2 Methods

2.2.1 Calibration profiles

A set of C_d vs. h/d_t calibration profiles were obtained using a non-porous substrate for use in estimating deposit thickness. A stainless steel sheet was fixed into the test section in place of the membrane, and C_d measurements were made for a set of known values of h/d_t. When running the FDG system using membranes, an added complication was that due to minor deformations in the supporting mesh and the impact of trans-membrane pressure, the position of the membrane surface relative to the gauge nozzle at a fixed position, h_0, was slightly different in each experiment. Contact between the nozzle and the membrane may damage the membrane, so a similar method as used for thickness estimations, in which such contact was avoided, was implemented to calibrate h_0 readings. Earlier experiments (detailed elsewhere [25]) have shown that TMP and Re_{duct} have a negligible effect on the shape of C_d vs. h/d_t profiles.

2.2.2 Thickness and strength estimation of preformed yeast cakes

Membranes were wetted with RO water before their installation into the test section. Degassed RO water was circulated through the system under the desired operating conditions until a steady-state flux was reached, during which time permeate was recycled back to the feed tank. This steady-state value was used as an estimation of the initial permeate flux. Fouling experiments were run at two different trans-membrane pressures (35 mbar and 50 mbar), both at a duct flow rate of 0.9 $L \cdot min^{-1}$ (Re_{duct} = 1000). These conditions were set, and the foulant was added as a powder to the feed tank under conditions of constant mixing. The gauge nozzle was maintained > 10 mm from the membrane surface to avoid disturbance to the fouling process. Fouling was allowed to proceed at constant TMP for 30 minutes, at which point a quasi-steady-state flux was reached whereby the particle deposition was balanced by detachment from the cake layer due to shear stress imposed by cross-flow velocity. Flux was monitored, and TMP was maintained using valve V2 (figure 4a). Permeate was not recycled to the feed tank.

The yeast deposit formed on the membrane was then tested using FDG. The gauging flow, m_g, was set to 0.2 $g \cdot s^{-1}$, and the gauge lowered towards the fouling layer, making continual

C_d measurements until an estimated clearance where $h/d_t \leq 0.25$ was reached. Thickness estimates were made at decreasing values of h_0 (the distance between the nozzle and the membrane) at 20 μm intervals in order to test the deformation behaviour of the deposit under a range of fluid shear stresses ($\tau_{w,\,max}$). The level of deformation (i.e. the reduction in deposit thickness) for each reading could then be used to indicate the strength of the cake at different thicknesses.

2.2.3 Thickness tracking of developing cake layer

Using the same preparation methods as described above, the membrane was installed into the test section, and a quasi-steady-state pure water flux was established. The gauging flow, m_g, was set to 0.2 g·s^{-1} and the gauge located at a position above the membrane such that $h/d_t = 0.2$ (where $h = h_0$ at time $t = 0$) before the foulant was added. Filtration conditions were set and the foulant added as powder to the constantly mixed tank. Cake growth was tracked by two different methods:

M1. The gauge was raised as cake growth proceeded in order to maintain $h/d_t \approx 0.2$, and thickness estimates were made continually. In this method the level of accuracy and applied fluid shear stress on the cake surface due to gauging flow is approximately constant.

M2. The gauge was kept at a single position, i.e. h_0 was kept constant, at a position where $h/d_t = 0.3$ prior to fouling (when $h = h_0$), and thickness estimates were made continually. By not moving the gauge during thickness tracking, less error was incurred due to height adjustments, however because the distance between the nozzle and the deposit, h, was decreasing due to deposit growth, the needle valve needed to be adjusted to maintain a gauging flow of 0.2 g·s^{-1}. This also meant that there was less scatter in the data as cake thickness increased.

A single set of fouling conditions was used for both of these protocols, where TMP = 35 mbar and $Re_{duct} = 1000$.

3. Results and Discussion

3.1 Calibration data

C_d vs. h/d_t profiles were produced from measurements over a stainless steel plate to which a curve, shown in figure 6, was fitted using a least squares method, defined by:

$$C_d = Ae^{-B\left(\frac{h}{dt}\right)} + Ce^{-D\left(\frac{h}{dt}\right)} \quad (6)$$

where A, B, C and D are constants of values 0.3775, 0.03293, -0.9347, and -14.11 respectively. The R^2 value was 0.9988 and the sum of squares due to error (SSE) was 0.001805. All yeast cake thickness estimates in this work were made by interpolating from this curve. Good agreement was found between this profile and data gathered during pure water filtration under the experimental conditions of this study, as shown in figure 6. Data were taken both in advancing and retreating mode (wherein the gauge was moved progressively closer to and away from the surface respectively). Little hysteresis was observed between the two, which is to be expected as readings were taken at steady state and should be unaffected by previous gauge movements.

3.2 Analysis of preformed yeast cakes

The majority of flux decline occurred during the first 60 seconds of filtration for all experiments. Flux decline is demonstrated by a drop in relative flux, *J'*, as given by:

$$J' = \frac{J}{J_0} \quad (7)$$

where J_0 is the initial flux at the start of the filtration. Typical flux decline curves observed during yeast fouling are shown in figure 7. Initial flux for a TMP of 50 mbar was around 20 000 $L \cdot m^{-2} \cdot h^{-1}$ and around 15 000 $L \cdot m^{-2} \cdot h^{-1}$ for a TMP of 35 mbar. In both cases a steady-state flux of 85 $L \cdot m^{-2} \cdot h^{-1}$ was reached after 30 minutes of fouling.

SEM micrographs taken of both virgin and fouled membranes are shown in figure 8. Samples of a virgin membrane were wetted prior to preparation. Fouled membrane samples were produced by filtration of the yeast suspension described in section 2.2.1 at a TMP of 50 mbar and Re_{duct} of 1000 for 30 minutes. All samples were freeze-dried in liquid nitrogen and cross sections were taken where the membrane had fractured during this process. Samples were sputter-coated with gold before analysis using a *JEOL JSM6480LV* electron microscope. The fouling layer broke away from the membrane during sample preparation, as shown in figure 8b, however upon closer inspection (figure 8c) a thin layer of yeast cells embedded into the surface of the membrane was identified. A sample of fouled membrane was rinsed with RO water and also examined using SEM. There was no evidence of yeast cells or debris on the surface or in the pores, indicating that all fouling was reversible.

Cake thicknesses of approximately 255 and 250 μm were identified for fouling runs at TMPs of 35 and 50 mbar respectively. Thickness estimates made in the region $0.25 < h/d_t \leq 0.35$ however, for which there was a high degree of scatter, indicated values possibly exceeding 1000 μm, which was corroborated by SEM images as well (figure 8c). In the current set-up, FDG flow deforms more fragile cakes even at the maximum allowable h/d_t value of 0.2, at which clearance $\tau_{w,\,max} = 10$ N·m^{-2}. Theoretically, accurate thickness measurements for preformed cakes are only possible where the stress imposed on the cake by the gauge is exceeded by that due to flow through the duct.

FDG analysis of the cake showed that its cohesive strength (i.e. the fluid shear required to separate cells/aggregates from the cake) increased further towards the surface of the membrane. Tangential shear stress on the surface of the cake was increased incrementally by gradually moving the gauge towards it, removing some of the foulant from the surface in the process. As more foulant was removed and the thickness decreased, the gauge nozzle was able to approach the surface of the cake more closely without causing deformation. Figure 9 shows the relationship between deposit thickness, δ, and maximum shear stress exerted by the gauge, $\tau_{w,\,max}$, for the two conditions studied. A near constant negative gradient between thickness and imposed shear stress is observed between 10 and 30 N·m^{-2}, indicating that cohesive strength (i.e. the fluid shear required to separate cells/aggregates from the cake) increased closer to the surface of the membrane. When the cake layer was > 200 μm, the uncertainties in the thickness and strength measurements were significant. This suggests that the layer at distance > 200 μm from the membrane is weak. It is worth noting that with the current FDG set up, the minimum detectable strength value is approximately 5 N·m^{-2}. Improvements to the FDG device are currently being made to allow more accurate measurements of weaker layers. Little or no further deformation was observed under shear stresses > 30 N·m^{-2}, with remaining layers < 100 μm thickness observed using FDG. This suggests a more persistent layer of particles on the surface of the membrane, held firmly against it by permeate flow through the membrane pores. The embedded layer of yeast cells in the membrane identified by SEM analysis (figure 8c) also confirms the presence of this layer, although the thickness indicated by FDG was larger than that imaged by electron microscopy. Complete removal of this persistent layer by FDG was not possible under these experimental conditions. The thicknesses estimated for these layers were 80 and 30 μm for TMPs of 35 and 80 mbar respectively. The difference is marginal, at approximately 9 cells thick (based on the average cell diameter of 5.8 μm), and aggregates larger than this were observed in particle size analysis of the suspension. The presence of aggregates may also contribute to the data scatter in figure 9, as it is unlikely that particles were removed by the gauge in single monolayers of cells. Small fluctuations in estimated thickness over time were

also noted whilst the gauge was in use which can be attributed in part to particle movements across the surface of the cake, as has been observed by Knutsen and Davis [33] for both yeast cells and latex microspheres.

Recovery of the fouled membrane from the test section confirmed that erosion of the fouling layer was localised to the area just beneath the gauge nozzle, forming a shallow crater, as shown in figure 10 (a and b). Visual inspection confirmed that from edge to edge this measured 1.8 mm, however there was some taper evident between the top of the undisturbed layer and the bottom of the crater. This tapered area closely matches the distance *s* between the inner and outer edges of the nozzle rim, where the bottom of the crater has a diameter corresponding to that of the orifice, d_t. The shape of the crater in figure 10b, and its relation to the gauge geometry (shown in figure 1) is expressed as a cross-section in figure 10c. This is consistent with the shear stress profile in the area underneath the gauge from figure 3 Although fluid shear stress decreases substantially at $r < d_t/2$, the disruption of the cake across the centre of the crater can be attributed to the suction of the gauge combined with the erosion of the surrounding material below the inner edge of the nozzle rim.

It is worth noting that the gauge also influenced the formation of the deposit downstream of the gauge, figure 10a shows two 'forks' emanating from the eroded region where the gauge was positioned. This is likely due to the effect of the gauge on downstream flow patterns in the duct. Streamline plots from preliminary CFD simulations by Lister et al. [20] have indicated some recirculation in this region just downstream of the gauge. Deposition behaviour and flow characteristics downstream of the gauge do not affect cake build up directly below it however.

3.3 Thickness tracking of developing cake layer

Cake layer thickness was estimated as it developed by constantly measuring Δp_{14} and m_g. Two different methods were employed, one in which the gauge clearance from the membrane, h_0, was manually adjusted to maintain $h/d_t \approx 0.2$ in line with increasing cake thickness, δ; and the other in which a constant value for $h_0$was used. Experimental conditions were: TMP = 35 mbar and Re_{duct} = 1000. A gauging flow of m_g = 0.2 g·s^{-1} was maintained in both cases.

3.3.1 *M1. Varying h_0*

Recorded h_0 values, corresponding h and δ estimates, and flux are shown against fouling time in figure 11. The trend seen for cake thickness corresponds well with the observed flux decline during the experiment, with growth of the yeast cake being initially very fast, estimated at around 0.77 μm·s^{-1}, and increasing asymptotically to a terminal value of *ca.* 130 μm. A high degree of scatter occurred in the first 60 seconds of fouling as the gauge height needed to be

adjusted often to maintain a constant clearance, *h*, from the cake, however as the growth rate decreased over time, h_0 adjustments were needed less regularly. Premature increases in h_0 also resulted in a higher degree of scatter, as indicated where h_0 is increased from 350 to 370 μm at around 1560 s. A maximum thickness of *ca.* 130 μm was identified at steady-state in this experiment, which indicates that the stresses imposed by FDG operation were too high to allow cake fouling to develop properly. Investigations using a smaller gauging flow rate (so as to reduce the applied shear stress) are currently underway.

3.3.2 *M2. Static h_0*

By performing this fouling experiment under the same conditions without adjusting h_0, it is possible to confirm that the cake growth observed by the previous method is independent of the gauge clearance. Thickness estimates using this method are shown in figure 12, demonstrating similar growth characteristics to those in figure 11. A similar asymptotic thickness of *ca.* 130 μm was identified, and the initial growth rate also showed good agreement, approximating to 0.84 $\mu m \cdot s^{-1}$. Further experiments using this method were performed at different initial clearances, where $h/d_t = 0.26$ and $h/d_t = 0.35$ (results not shown in this paper). At higher initial clearances, thickness estimates of the cake cannot be made to a satisfying degree of accuracy until it has increased to a point at which $h/d_t \leq 0.2$. If the clearance is too low however, cake growth will be further hindered by the increased shear forces imposed by the gauge.

3.3.3 Modelling cake development

It is worth noting that although the cake growth can be tracked with time, the final cake thickness estimated using FDG in this case is not a true representation of the cake thickness across the whole membrane surface; but an approximation of cake growth under the fluid shear conditions imposed by the gauge. Cake fouling appears to start immediately, but increases only to a limiting thickness of 130 μm, above which FDG measurements disrupt cake formation. Recovery of the membrane following both experiments showed that the presence of the gauge above the membrane during fouling had significantly affected particle deposition, evidenced by similar ‘forks’ to those in figure 10a. The effect of FDG on cake layer formation is governed by the properties of the feed suspension, and this effect has not been observed in similar studies [20, 21] in which monodisperse suspensions were filtered. Asymptotic thickness measurements during fouling and the thickness measurements of preformed layers may become more similar when filtering less aggregated yeast suspensions.

Because a complex suspension containing large aggregates was filtered, and FDG technique can influence cake formation, it is important to determine that it is driven by

membrane flux rather than settling or diffusion towards the membrane surface. For this purpose, a simple approximation is deemed sufficient, in which mass transfer coefficients for convection, diffusion and settling are derived. Epstein [34] gave the following equation to describe particle transport from bulk fluid to a surface:

$$\frac{dM}{dt} = k_t(C_b - C_w) \tag{8}$$

where M is the mass of particles per unit area of the surface, C_b and C_w are the concentrations of particles in the bulk fluid and at the wall respectively, and k_t is the transport coefficient. In this case C_w is taken to be the concentration at the surface of the membrane, assumed to be zero initially. Equation (8) can then be expressed in terms of initial cake growth:

$$\frac{dM}{dt} = \rho_p(1-\varepsilon)\frac{d\delta}{dt} = k_t C_b \tag{9}$$

where ρ_p is the density of foulant particles, and ε is the voidage of the cake (assumed constant at a value of 0.4, for densely packed spheres [35]). For the purposes of this approximation it is assumed that this initial growth rate is representative of that across the entire area of the membrane. Using a value of ρ_p = 1130·kg·m^{-3}[36], and the average growth rate (from figures 11 and 12):

$$\frac{d\delta}{dt} = 0.81\ \mu m \cdot s^{-1}$$

gives a value for k_t of 5.49×10^{-4} m·s^{-1}.

A corresponding mass transport coefficient, k_m, can be derived, representing particle transport due to convective diffusion in a flowing duct. This is given in terms of the Sherwood number, *Sh*, and hydraulic diameter, d_H, for the duct (in this case d_H is equal to the width of the duct, D = 15 mm) [27]:

$$k_m = \frac{D_p Sh}{d_H} \tag{10}$$

where D_p is the particle diffusivity. The Stokes-Einstein equation (which implicitly assumes non-slip conditions on the particle's surface) can be used to approximate diffusion of large spherical molecules or suspended particles in fluids of low molecular weight [37]:

$$D_p = \frac{k_b T}{3\mu\pi d_p} \tag{11}$$

where k_b is the Boltzmann constant ($1.38 \times 10^{-23} m^2 \cdot kg \cdot s^{-2} \cdot K^{-1}$), T and μ are the fluid temperature and viscosity respectively, and d_p is the diameter of a single yeast cell (a worst case scenario subtending to the maximum possible diffusivity). The Sherwood number can be estimated using the Sieder-Tate correlation for laminar flow [37]:

$$Sh = 1.86 {Re_{duct}}^{1/3} Sc^{1/3} \left(\frac{D}{L}\right)^{1/3} \tag{12}$$

where L is the length of the membrane surface, and the Schmidt number, Sc, is given by:

$$Sc = \frac{\mu}{\rho D_p} \tag{13}$$

Using equations (10) to (13) gives a value of $k_m = 9.87 \times 10^{-9}$ m·s^{-1}, over 4 orders of magnitude lower than the transport coefficient k_t derived from the initial growth rate.

A crude approximation for the rate of particle settling is also produced for comparison with the estimated cake growth. A settling coefficient analogous to the transport coefficient in equation (8), k_s, taking the polydispersity of the suspension into account, is calculated as follows:

$$k_s = \sum x_i u_{t,i} \tag{14}$$

where x_i is the %volume of particles of size i and $u_{t,i}$ is the terminal velocity (for creeping flow) of a particle of diameter $d_{p,i}$, given by Stokes law [38]:

$$u_{t,i} = \frac{(\rho - \rho_p) d_{p,i}^2 g}{\mu} \tag{15}$$

where g is the gravitational constant. Due to the low volume fraction of particles in the suspension, estimation of hindered settling velocity using the Richardson-Zaki equation or other expressions based on volume fraction would yield an almost identical value to terminal velocity.

For this reason, and to estimate for a worst case scenario, terminal velocity for cells/aggregates is used in equation (14). The resulting settling coefficient, k_s, was 8.45×10^{-5} m·s^{-1}, which indicates that over 15% of cake deposition may be due to particle settling. The majority of settling however (>90%), can be attributed to aggregates larger than 100 µm diameter, and less than 1% is due to those in the range of single cells.

By comparison of the transport coefficients for diffusion and settling (k_m and k_s respectively) with that derived from the initial cake growth rate (k_t):

$$k_t = 5.49 \times 10^{-4}\ \text{m·s}^{-1},$$

$$k_m = 9.87 \times 10^{-9}\ \text{m·s}^{-1} \ll k_t,$$

$$k_s = 8.45 \times 10^{-5}\ \text{m·s}^{-1} \approx 0.15 k_t$$

it is clear that cake growth is primarily governed by filtration. Particle settling has a marked impact on cake growth, mainly due to presence of large aggregates. This may also contribute to the difference between terminal cake thickness measured after fouling (as detailed in section 3.1) and during fouling (as detailed in section 3.2). The impact of particle settling upon FDG analysis in membrane filtration will be subject to further investigation.

4. Conclusion

The technique of fluid dynamic gauging has been used to estimate the thickness and strength of fouling layers during the microfiltration of a non-ideal suspension of polydisperse yeast particles, which included single cells and large aggregates. The strength of pre-developed fouling deposits (cakes) was assessed by applying controlled fluid shear stress to the surface of the cake and measuring the resulting deformation. The resilience of the cake to fluid shear was found to be inversely proportional to cake thickness, down to a level where a persistent layer, less than 100 µm thick and capable of withstanding stresses outside of the operating limits of the gauge, remained. At a thickness of > 250 µm, these cakes were found to be easily deformable, with particles removed from the cake under shear stresses below 10 N·m^{-2}. Accurate gauge measurements at shear stresses lower than this were not possible in these studies.

Thickness estimates for a developing cake layer were also performed, from which initial cake growth was estimated. The asymptotic rate of cake growth was found to correspond well with the decreasing rate of flux decline. The overall accuracy of thickness estimates in these studies was ± 5 µm to ± 20 µm, with lower error margins at gauge positions closer to the cake (which correspond also to higher imposed shear stresses). Consideration of both settling phenomena and convective diffusion confirmed that cake growth was governed mainly by convection of particles towards the membrane due to filtration.

Work on pressure mode FDG in membrane systems is on-going, and further studies on the behaviour of yeast cakes under applied fluid shear are planned. One of the greatest strengths of the FDG technique is its versatility, in that it can be applied to a wide range of both ideal and non-ideal foulants. With a little further development it should be possible to study a wide range of feeds and membrane types, specific to industrial processes. The effects anti-fouling measures such as feed pre-treatment and surface modification on the rate of cake formation and its removal properties could be investigated on-the-fly, without prerequisite data for, or modification of the feed.

Acknowledgements

We would like to thank both Mr Zlatko Saracevic of the University of Cambridge for providing assistance with particle sizing studies, and also the Engineering and Physical Sciences Research Council (EPSRC) for providing financial support.

Appendix

A1. Error calculations

The following equation is use to estimate error in C_d calculations:

$$\frac{\delta C_d}{C_d} = \sqrt{\left(\frac{\delta m_g}{m_g}\right)^2 + \left(\frac{1}{2}\frac{\delta \rho}{\rho}\right)^2 + \left(\frac{1}{2}\frac{\delta \Delta P_{13}}{\Delta P_{13}}\right)^2} \qquad \text{(A1)}$$

from which the error in thickness estimates, δ, can be made for each individual reading. Due to the nature of the calibration profile shown in figure 6, the error margin is greater where h/d_t is higher. For a value of $h/d_t = 0.2$, the error in thickness measurements was calculated to be ± 10 μm.

References

[1] Z.F. Cui, H.S. Muralidhara, Membrane technology: a practical guide to membrane technology and applications in food and bioprocessing, Elsevier/Butterworth-Heinemann, Amsterdam ; London, 2010.
[2] Anon., US membrane separation technology markets analysed, Membrane Technology, 2002 (2000) 10-12.
[3] W.D. Mores, R.H. Davis, Direct visual observation of yeast deposition and removal during microfiltration, Journal of Membrane Science, 189 (2001) 217-230.
[4] W.D. Mores, R.H. Davis, Direct observation of membrane cleaning via rapid backpulsing, Desalination, 146 (2002) 135-140.
[5] W.D. Mores, R.H. Davis, Yeast foulant removal by backpulses in crossflow microfiltration, Journal of Membrane Science, 208 (2002) 389-404.

[6] H. Li, A.G. Fane, H.G.L. Coster, S. Vigneswaran, Direct observation of particle deposition on the membrane surface during crossflow microfiltration, Journal of Membrane Science, 149 (1998) 83-97.
[7] H. Li, A.G. Fane, H.G.L. Coster, S. Vigneswaran, An assessment of depolarisation models of crossflow microfiltration by direct observation through the membrane, Journal of Membrane Science, 172 (2000) 135-147.
[8] H. Li, A.G. Fane, H.G.L. Coster, S. Vigneswaran, Observation of deposition and removal behaviour of submicron bacteria on the membrane surface during crossflow microfiltration, Journal of Membrane Science, 217 (2003) 29-41.
[9] T. Schluep, F. Widmer, Initial transient effects during cross flow microfiltration of yeast suspensions, Journal of Membrane Science, 115 (1996) 133-145.
[10] J. Altmann, S. Ripperger, Particle deposition and layer formation at the crossflow microfiltration, Journal of Membrane Science, 124 (1997) 119-128.
[11] J. Mendret, C. Guigui, P. Schmitz, C. Cabassud, P. Duru, An optical method for in situ characterization of fouling during filtration, AIChE Journal, 53 (2007) 2265-2274.
[12] J. Li, R.D. Sanderson, In situ measurement of particle deposition and its removal in microfiltration by ultrasonic time-domain reflectometry, Desalination, 146 (2002) 169-175.
[13] S.K. Sikder, M.B. Mbanjwa, D.A. Keuler, D.S. McLachlan, F.J. Reineke, R.D. Sanderson, Visualisation of fouling during microfiltration of natural brown water by using wavelets of ultrasonic spectra, Journal of Membrane Science, 271 (2006) 125-139.
[14] X. Xu, J. Li, H. Li, Y. Cai, Y. Cao, B. He, Y. Zhang, Non-invasive monitoring of fouling in hollow fiber membrane via UTDR, Journal of Membrane Science, 326 (2009) 103-110.
[15] D. Hughes, U.K. Tirlapur, R. Field, Z. Cui, In situ 3D characterization of membrane fouling by yeast suspensions using two-photon femtosecond near infrared non-linear optical imaging, Journal of Membrane Science, 280 (2006) 124-133.
[16] S. Buetehorn, L. Utiu, M. Küppers, B. Blümich, T. Wintgens, M. Wessling, T. Melin, NMR imaging of local cumulative permeate flux and local cake growth in submerged microfiltration processes, Journal of Membrane Science, 371 (2011) 52-64.
[17] V. Chen, H. Li, A.G. Fane, Non-invasive observation of synthetic membrane processes - a review of methods, Journal of Membrane Science, 241 (2004) 23-44.
[18] Y.M.J. Chew, W.R. Paterson, D.I. Wilson, Fluid dynamic gauging: A new tool to study deposition on porous surfaces, Journal of Membrane Science, 296 (2007) 29-41.
[19] S.A. Jones, Y.M.J. Chew, M.R. Bird, D.I. Wilson, The application of fluid dynamic gauging in the investigation of synthetic membrane fouling phenomena, Food and Bioproducts Processing, 88 (2010) 409-418.
[20] V.Y. Lister, C. Lucas, P.W. Gordon, Y.M.J. Chew, D.I. Wilson, Pressure mode fluid dynamic gauging for studying cake build-up in cross-flow microfiltration, Journal of Membrane Science, 366 (2011) 304-313.
[21] S.A. Jones, Y.M.J. Chew, D.I. Wilson, M.R. Bird, Fluid dynamic gauging of microfiltration membranes fouled with sugar beet molasses, Journal of Food Engineering, 108 (2012) 22-29.
[22] J.Y.M. Chew, W.R. Paterson, D.I. Wilson, Fluid dynamic gauging for measuring the strength of soft deposits, Journal of Food Engineering, 65 (2004) 175-187.
[23] J.Y.M. Chew, W.R. Paterson, D.I. Wilson, V. Höufling, W. Augustin, A Method for Measuring the Strength of Scale Deposits on Heat Transfer Surfaces, Developments in Chemical Engineering and Mineral Processing, 13 (2005) 21-30.
[24] T.R. Tuladhar, W.R. Paterson, N. Macleod, D.I. Wilson, Development of a novel non-contact proximity gauge for thickness measurement of soft deposits and its application in fouling studies, Can. J. Chem. Eng., 78 (2000) 935-947.
[25] P. Schmitz, M. Prat, 3-D Laminar stationary flow over a porous surface with suction: Description at pore level, AIChE Journal, 41 (1995) 2212-2226.
[26] W. Lewis, J. Chew, M.R. Bird, Experimental and CFD Studies of Fluid Dynamic Gauging in Cross-Flow Microfiltration Systems, in: P.S. Taoukis, N.G. Stoforos, V.T. Karathanos, G.D.

Saravacos (Eds.) 11th International Congress of Engineering and Food (ICEF11), Cosmosware, Athens, Greece, 2011, pp. 375-376.
[27] S. Middleman, An introduction to fluid dynamics : principles of analysis and design, Wiley, New York ; Chichester, 1998.
[28] T. Gu, Y.M.J. Chew, W.R. Paterson, D.I. Wilson, Experimental and CFD studies of fluid dynamic gauging in duct flows, Chemical Engineering Science, 64 (2009) 219-227.
[29] T.R. Tuladhar, W.R. Paterson, D.I. Wilson, Dynamic gauging in duct flows, Can. J. Chem. Eng., 81 (2003) 279-284.
[30] M.A. Malone, Jr., Infrared Microspectroscopy: A Study of the Single Isolated Bread Yeast Cell, Thesis (MSc), Ohio State University, Columbus, 2010.
[31] G. Guillemot, G. Vaca-Medina, H. Martin-Yken, A. Vernhet, P. Schmitz, M. Mercier-Bonin, Shear-flow induced detachment of Saccharomyces cerevisiae from stainless steel: Influence of yeast and solid surface properties, Colloids and Surfaces B: Biointerfaces, 49 (2006) 126-135.
[32] R.G.M. van der Sman, H.M. Vollebregt, A. Mepschen, T.R. Noordman, Review of hypotheses for fouling during beer clarification using membranes, Journal of Membrane Science, 396 (2012) 22–31.
[33] J.S. Knutsen, R.H. Davis, Deposition of foulant particles during tangential flow filtration, Journal of Membrane Science, 271 (2006) 101-113.
[34] N. Epstein, Particulate fouling of Heat Transfer Surfaces: Mechanisms and Models, in: L.F. Melo, T.R. Bott, C.A. Bernardo (Eds.) Fouling science and technology : Advanced study institute on advances in fouling science and technology : Papers, Kluwer Academic, Dordrecht ; Boston, 1988.
[35] J.F. Richardson, J.H. Harker, J.R. Backhurst, Particle technology and separation processes, Butterworth-Heinemann, Amsterdam; Boston, 2007.
[36] M. Meireles, C. Molle, M.J. Clifton, P. Aimar, The origin of high hydraulic resistance for filter cakes of deformable particles: cell-bed deformation or surface-layer effect?, Chemical Engineering Science, 59 (2004) 5819-5829.
[37] R.B. Bird, W.E. Stewart, E.N. Lightfoot, Transport phenomena, 2nd rev. ed. ed., J. Wiley, New York ; Chichester, 2007.
[38] C. Orr, Particulate technology, Macmillan ; London : Collier-Macmillan, New York, 1966.

List of Figures

Figure 1. Schematic of FDG nozzle, where for this research: $d = 4$ mm, $d_t = 1$ mm, $s = 0.5$ mm, and $\alpha = 30°$. Stations 1 to 4 represent locations in the system between which important pressure differences would be observed.

Figure 2. Typical calibration data at known h_0 clearance values over a non-porous, stainless steel substrate at a gauging flowrate, m_g, of 0.2 $g \cdot s^{-1}$ and static pressure, Δp_s, of 35 mbar. Open symbols – C_d (left axis), closed symbols – Δp_{13} (right axis). The dashed vertical line represents the transition (at $h/d_t = 0.25$) between the incremental and asymptotic zones.

Figure 3. Preliminary CFD simulations of stress distribution on surface beneath the rim of the gauge nozzle during CFMF. Simulation conditions are $Re_{duct} = 1550$, $TMP = 35$ mbar, and $J = 60$ $Lm^{-2}h^{-1}$. Position of the gauging nozzle is shown by the distance s inside the vertical dotted lines. (□) – $h/d_t = 0.15$, (◊) – $h/d_t = 0.25$. Solid and dashed lines show the analytical solution from equation (3) for $h/d_t = 0.25$ and $h/d_t = 0.15$ respectively.

Figure 4. Schematics of apparatus (a) Rig set up, (b) FDG test section, NV – Needle Valve, PT – Pressure Tapping, FC – Flexible Coupling, Mi - Micrometer, X – X-Piece, SP – Spring, BP – Bleed Point, G – Gauge, M – Membrane, S – Stainless steel mesh support, RS – Rubber Seal. m_g and m_p represent gauging and permeate flow respectively Dimensions are in mm (not to scale).

Figure 5. Cell/aggregate size distribution for yeast suspension, open and closed symbols represent repeat experiments. Measurements were carried out using a *Coulter* LS230 Laser-diffraction particle sizer.

Figure 6. Symbols: C_d vs. h/d_t data for microfiltration of pure water at TMP = 35 mbar and $Re_{duct} = 1000$. Solid line: calibration curve defined by equation (5). Open symbols – retreating mode, closed symbols – advancing mode. Vertical dashed line represents the transition between incremental and asymptotic data. Thickness measurements cannot be made accurately using C_d values outside the incremental region.

Figure 7. Typical flux decline curves produced during fouling of 5 μm microfiltration membranes with 0.09 vol% yeast suspension: TMP = 50 mbar, dashed line: TMP = 35 mbar. $Re_{duct} = 1000$ for both conditions. Initial fluxes were 20 000 and 15 000 $L \cdot m^{-2} \cdot h^{-1}$ respectively.

Figure 8. SEM images of: (a) virgin membrane at 1000× magnification, (b) fouled membrane at fractured edge under 200 × magnification, (c) fouled membrane at fractured edge

under 1000× magnification. All images were recorded using 5 kV. Fouled membranes were produced by filtration of 0.09 vol% yeast suspension at TMP = 50 mbar and Re_{duct} = 1000 for 30 minutes.

Figure 9. Estimated cake thickness against maximum imposed fluid shear for a cake formed with Re_{duct} = 1000. Closed symbols – TMP = 50 mbar, Open symbols – TMP = 35 mbar.

Figure 10. (a) and (b) Photographs showing the crater formed by deformation of the cake by FDG during analysis of preformed layers. The width of the eroded region (1.8 mm) falls between the diameter of the nozzle throat, d_t, and the outside edge of the nozzle rim, $d_t/2 + s$, as shown in (c), a representation of the cross section of the crater, in which the shape corresponds to the overhead view in (b). Direction of flow is from left to right.

Figure 11. Thickness estimation and flux decline against time for a fouling run at TMP = 35 mbar and Re_{duct} = 1000. (×) h_0, (■) h, (▲) δ; the solid curve represents the relative flux (right axis) and the dotted line indicates the estimated initial growth rate of the cake.

Figure 12. Estimated cake thickness against time at TMP =35 mbar, Re_{duct} = 1000, for static h_0 values of 300 μm. (▲) estimated thickness δ, (⁎) static gauge position, h_0. The solid line shows the relative flux (right axis), and the dotted line indicates the estimated initial growth rate of the cake.

Figure 1. Schematic of FDG nozzle, where for this research: d = 4 mm, d_t = 1 mm, s = 0.5 mm, and α = 30°. Stations 1 to 4 represent locations in the system between which important pressure differences would be observed.

Figure 2. Typical calibration data at known h_0 clearance values over a non-porous, stainless steel substrate at a gauging flowrate, m_g, of 0.2 g·s^{-1} and static pressure, Δp_s, of 35 mbar. Open symbols – C_d (left axis), closed symbols – Δp_{13} (right axis). The dashed vertical line represents the transition (at h/d_t = 0.25) between the incremental and asymptotic zones.

Figure 3. Preliminary CFD simulations of stress distribution on surface beneath the rim of the gauge nozzle during CFMF. Simulation conditions are Re_{duct} = 1550, TMP = 35 mbar, and J = 60 L·m^{-2}·h^{-1}. Position of the gauging nozzle is shown by the distance s inside the vertical dotted lines. (□) – h/d_t = 0.15, (◊) – h/d_t = 0.25. Solid and dashed lines show the analytical solution from equation (3) for h/d_t = 0.25 and h/d_t = 0.15 respectively.

Figure 4. Schematics of apparatus (a) Rig set up, (b) FDG test section, NV – Needle Valve, PT – Pressure Tapping, FC – Flexible Coupling, Mi - Micrometer, X – X-Piece, SP – Spring, BP – Bleed Point, G – Gauge, M – Membrane, S – Stainless steel mesh support, RS – Rubber Seal. m_g and m_p represent gauging and permeate flow respectively Dimensions are in mm (not to scale).

Figure 5. Cell/aggregate size distribution for yeast suspension, open and closed symbols represent repeat experiments. Measurements were carried out using a *Coulter* LS230 Laser-diffraction particle sizer.

Figure 6. Symbols: C_d vs. h/d_t data for microfiltration of pure water at TMP = 35 mbar and Re_{duct} = 1000. Solid line: calibration curve defined by equation (5). Open symbols – retreating mode, closed symbols – advancing mode. Vertical dashed line represents the transition between incremental and asymptotic data. Thickness measurements cannot be made accurately using C_d values outside the incremental region.

Figure 7. Typical flux decline curves produced during fouling of 5 µm microfiltration membranes with 0.09 vol% yeast suspension: TMP = 50 mbar, dashed line: TMP = 35 mbar. Re_{duct} = 1000 for both conditions. Initial fluxes were 20 000 and 15 000 Lm^{-2}h^{-1} respectively.

Figure 8. SEM images of: (a) virgin membrane at 1000× magnification, (b) fouled membrane at fractured edge under 200 × magnification, (c) fouled membrane at fractured edge under 1000× magnification. All images were recorded using 5 kV. Fouled membranes were produced by filtration of 0.09 vol% yeast suspension at TMP = 50 mbar and Re_{duct} = 1000 for 30 minutes.

Figure 9. Estimated cake thickness against maximum imposed fluid shear for a cake formed with Re_{duct} = 1000. Closed symbols – TMP = 50 mbar, Open symbols – TMP = 35 mbar.

Figure 10. (a) and (b) Photographs showing the crater formed by deformation of the cake by FDG during analysis of preformed layers. The width of the eroded region (1.8 mm) falls between the diameter of the nozzle throat, d_t, and the outside edge of the nozzle rim, $d_t/2 + s$, as shown in (c), a representation of the cross section of the crater, in which the shape corresponds to the overhead view in (b). Direction of flow is from left to right.

Figure 11. Thickness estimation and flux decline against time for a fouling run at TMP = 35 mbar and Re_{duct} = 1000. (×) h_0, (■) h, (▲) δ; the solid curve represents the relative flux (right axis) and the dotted line indicates the estimated initial growth rate of the cake.

Figure 12. Estimated cake thickness against time at TMP =35 mbar, Re_{duct} = 1000, for static h_0 values of 300 μm. (▲) estimated thickness δ, (✱) static gauge position, h_0. The solid line shows the relative flux (right axis), and the dotted line indicates the estimated initial growth rate of the cake.

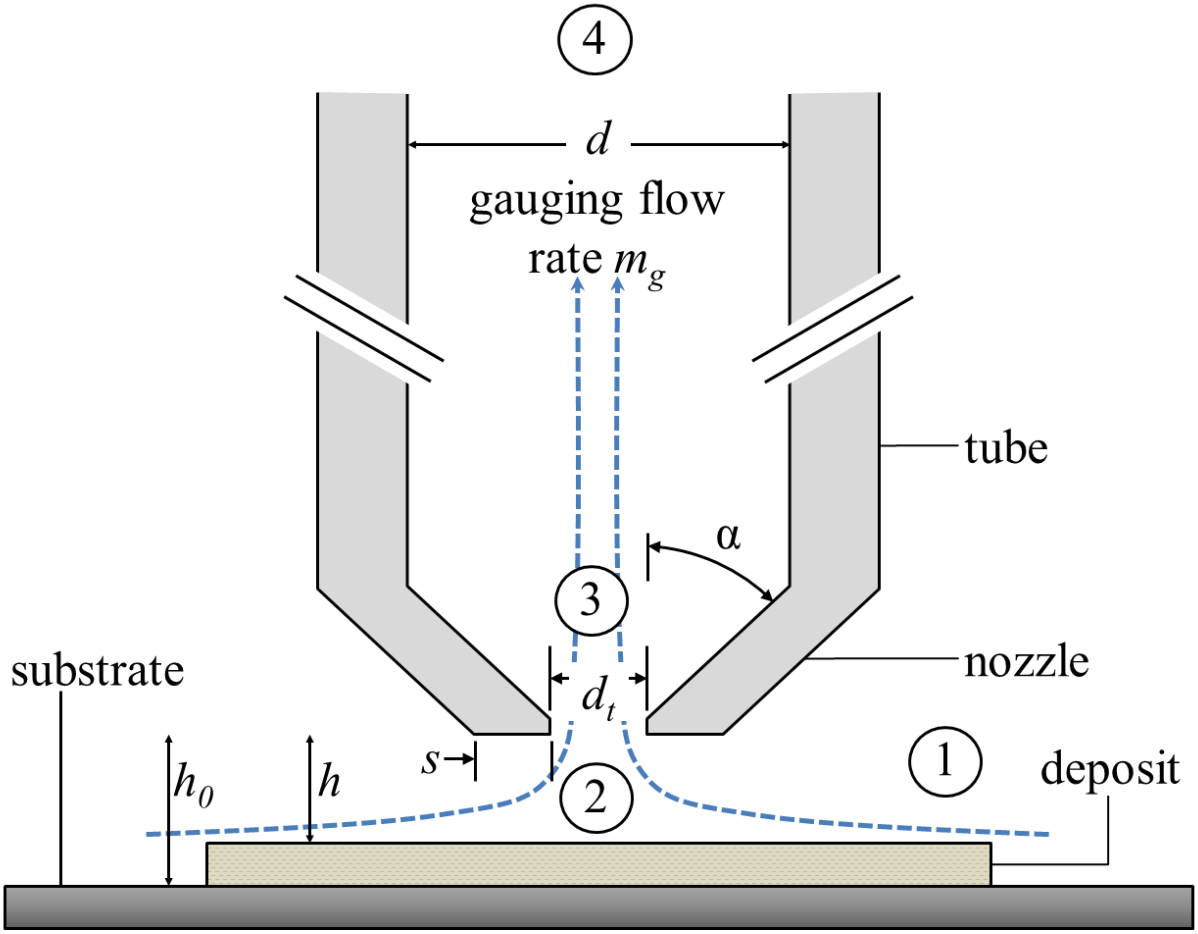

Figure 1. Schematic of FDG nozzle, where for this research: d = 4 mm, d_t = 1 mm, s = 0.5 mm, and α = 30°. Stations 1 to 4 represent locations in the system between which important pressure differences would be observed.

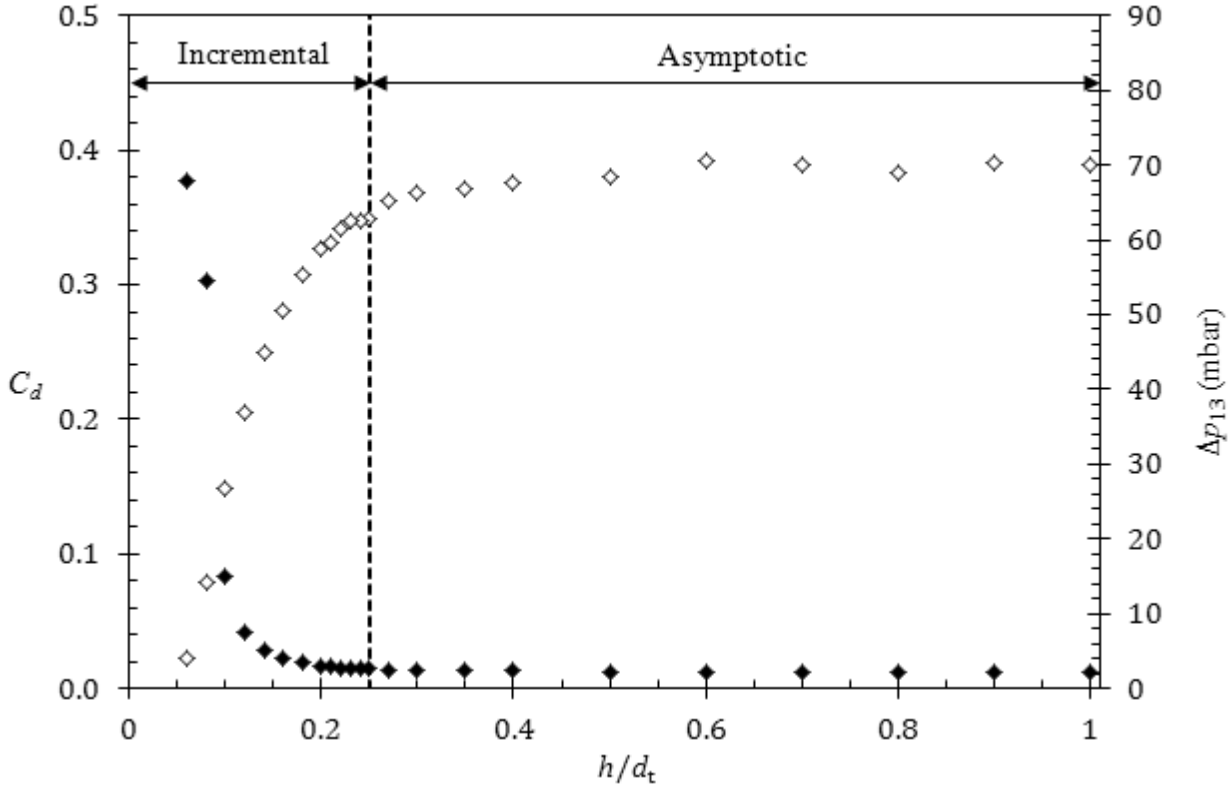

Figure 2. Typical calibration data at known h_0 clearance values over a non-porous, stainless steel substrate at a gauging flowrate, m_g, of 0.2 g·s^{-1} and static pressure, Δp_s, of 35 mbar. Open symbols – C_d (left axis), closed symbols – Δp_{13} (right axis). The dashed vertical line represents the transition (at $h/d_t = 0.25$) between the incremental and asymptotic zones.

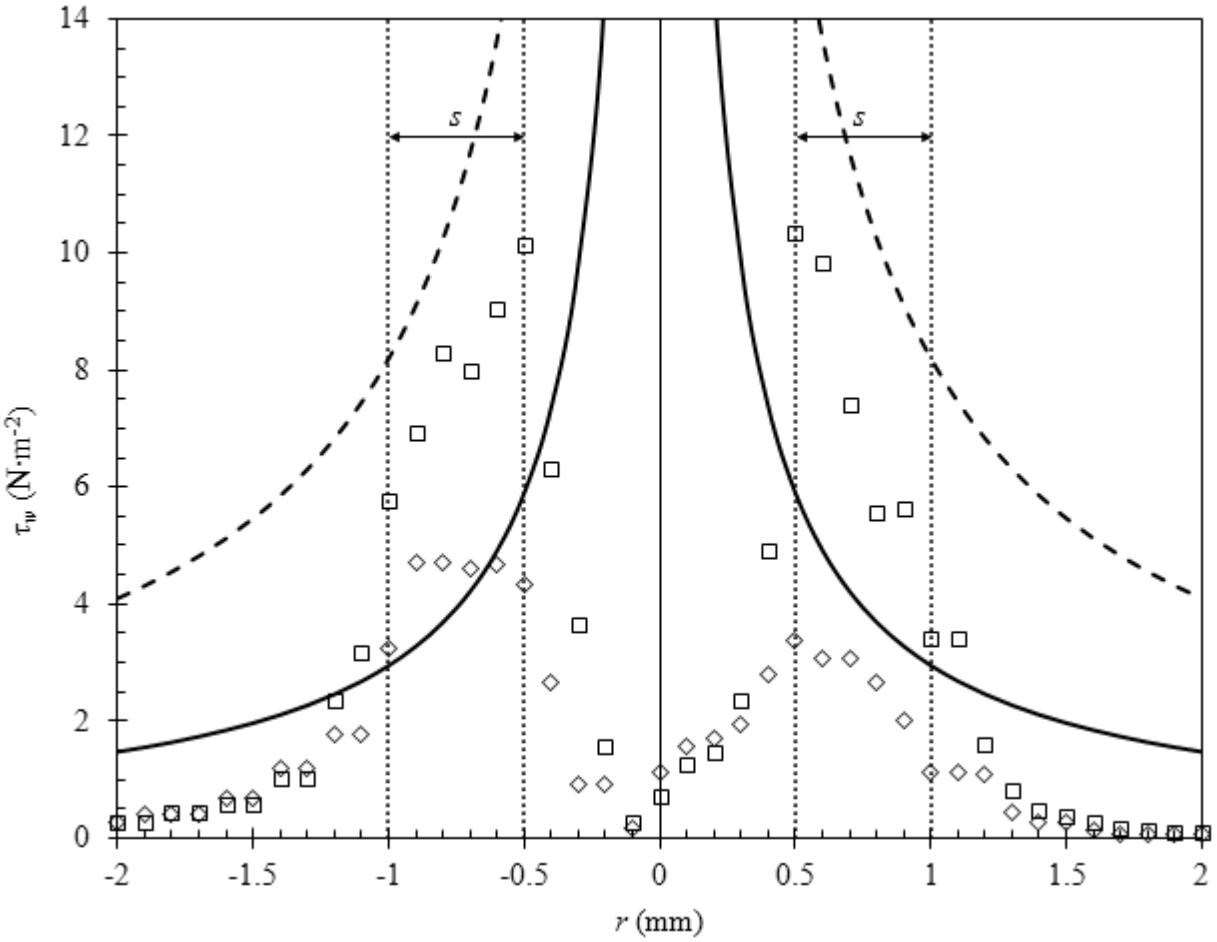

Figure 3. Preliminary CFD simulations of stress distribution on surface beneath the rim of the gauge nozzle during CFMF. Simulation conditions are Re_{duct} = 1550, *TMP* = 35 mbar, and J = 60 L·m^{-2}·h^{-1}. Position of the gauging nozzle is shown by the distance s inside the vertical dotted lines. (□) – h/d_t = 0.15, (◊) – h/d_t = 0.25. Solid and dashed lines show the analytical solution from equation (3) for h/d_t = 0.25 and h/d_t = 0.15 respectively.

(a)

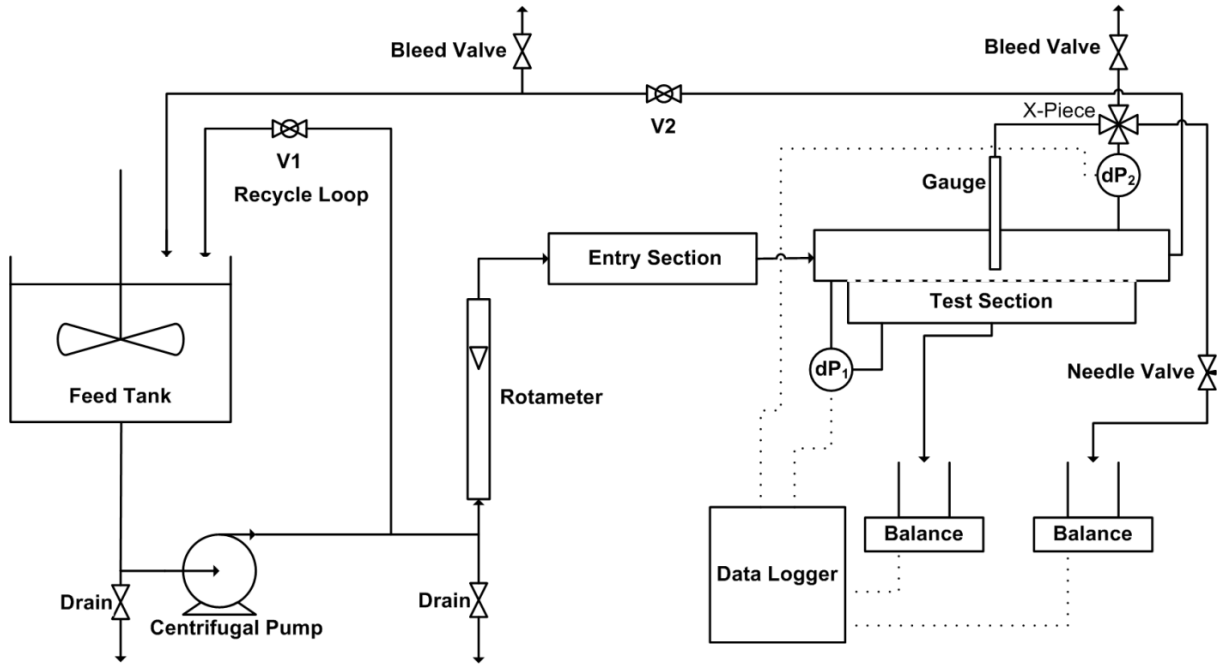
Bleed Valve
Bleed Valve
V2
X-Piece
V1
Recycle Loop
Gauge
dP2
Entry Section
Test Section
Feed Tank
Rotameter
dP1
Needle Valve
Balance
Balance
Data Logger
Drain
Centrifugal Pump
Drain

(b)

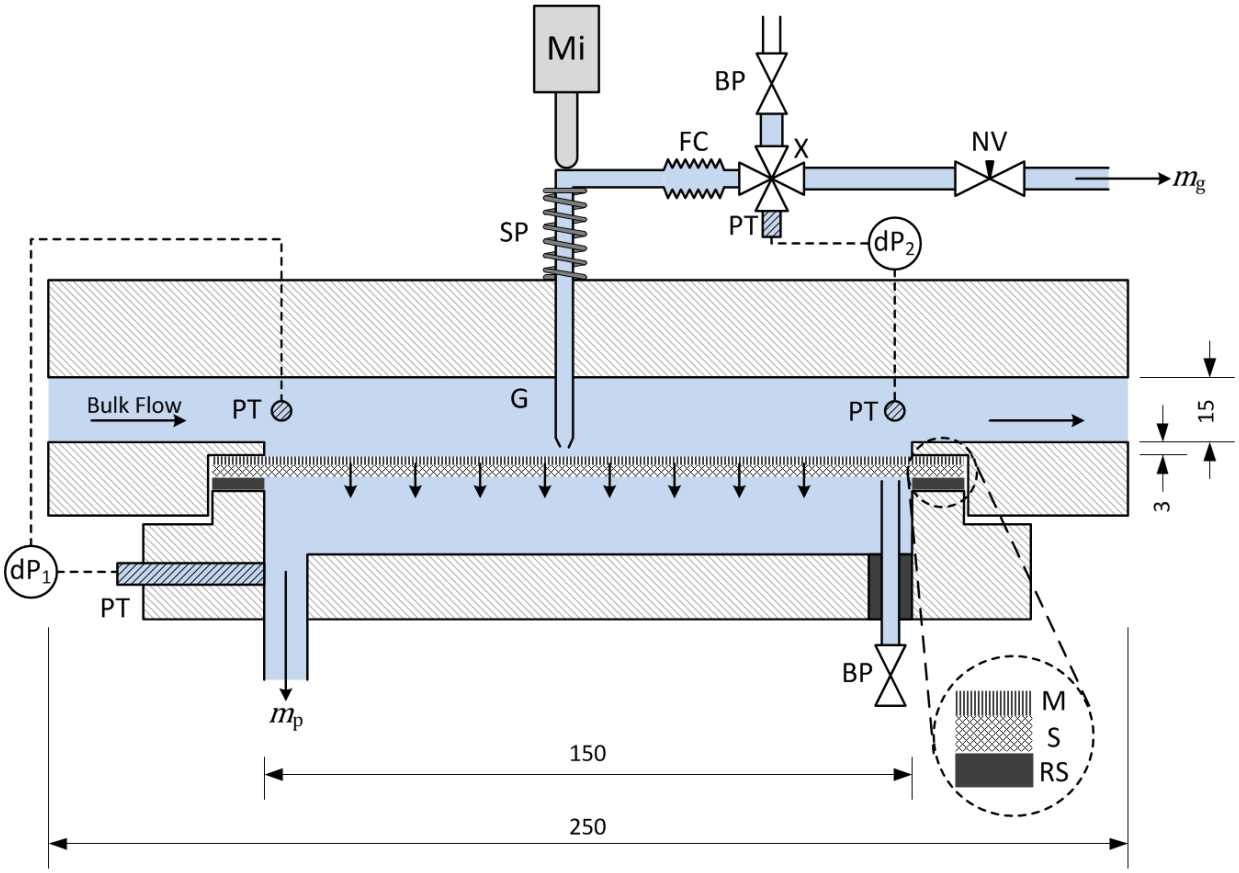
Mi
BP
FC
X
NV
mg
SP
PT
dP2
Bulk Flow
PT
G
PT
15
3
dP1
PT
BP
mp
M
S
RS
150
250

Figure 4. Schematics of apparatus (a) Rig set up, (b) FDG test section, NV – Needle Valve, PT – Pressure Tapping, FC – Flexible Coupling, Mi - Micrometer, X – X-Piece, SP – Spring, BP – Bleed Point, G – Gauge, M – Membrane, S – Stainless steel mesh support, RS – Rubber Seal. m_g and m_p represent gauging and permeate flow respectively Dimensions are in mm (not to scale).

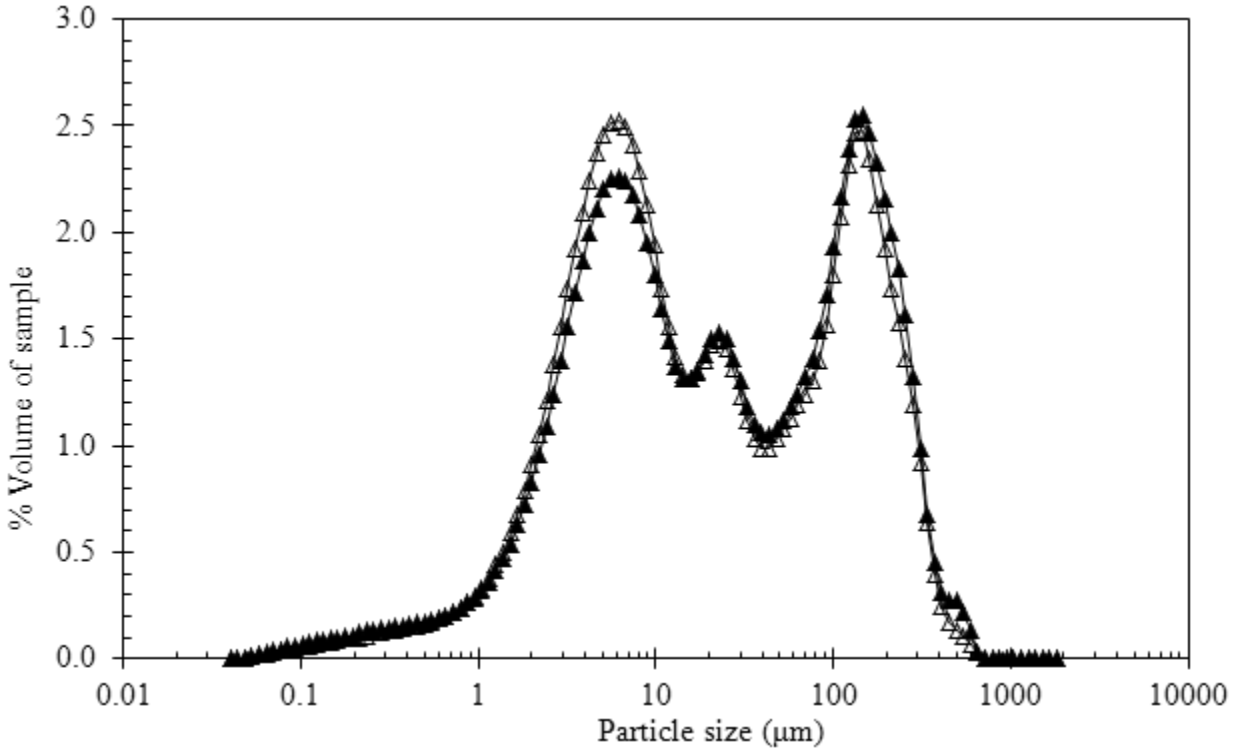

Figure 5. Cell/aggregate size distribution for yeast suspension, open and closed symbols represent repeat experiments. Measurements were carried out using a *Coulter* LS230 Laser-diffraction particle sizer.

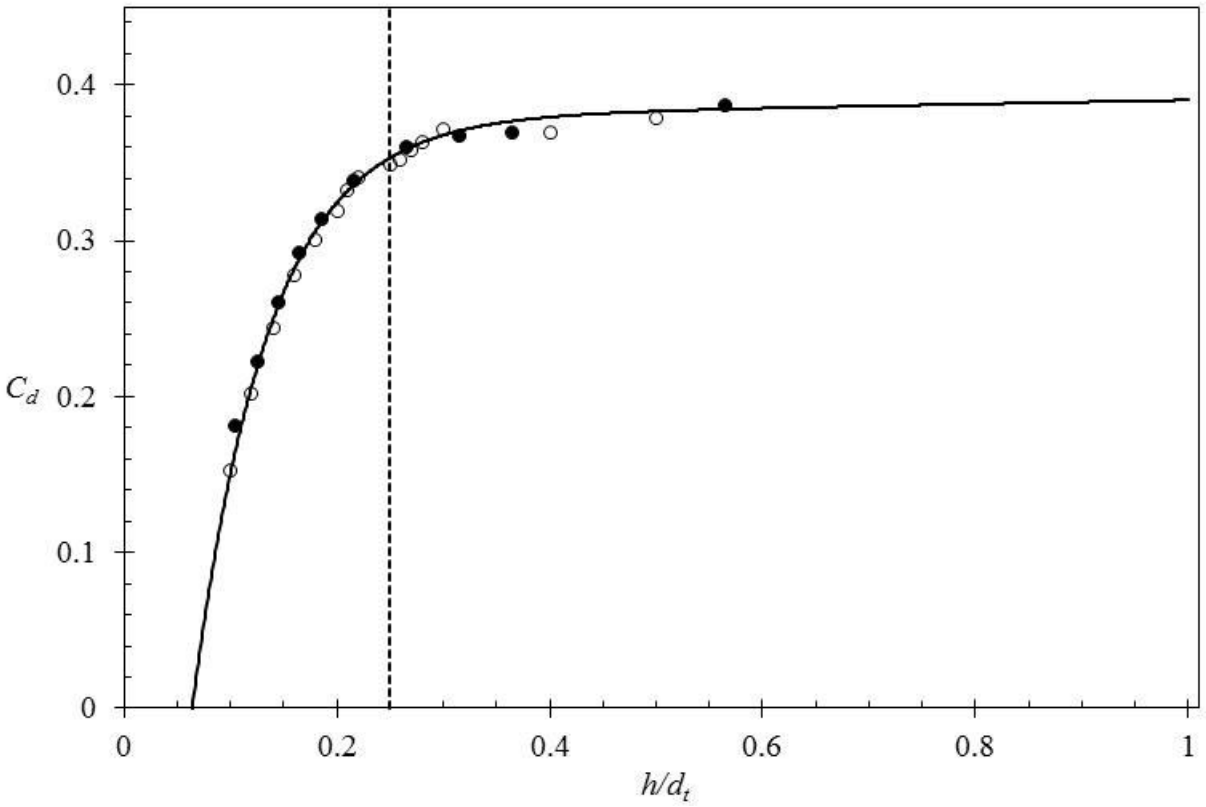

Figure 6. Symbols: C_d vs. h/d_t data for microfiltration of pure water at TMP = 35 mbar and Re_{duct} = 1000. Solid line: calibration curve defined by equation (5). Open symbols – retreating mode, closed symbols – advancing mode. Vertical dashed line represents the transition between incremental and asymptotic data. Thickness measurements cannot be made accurately using C_d values outside the incremental region.

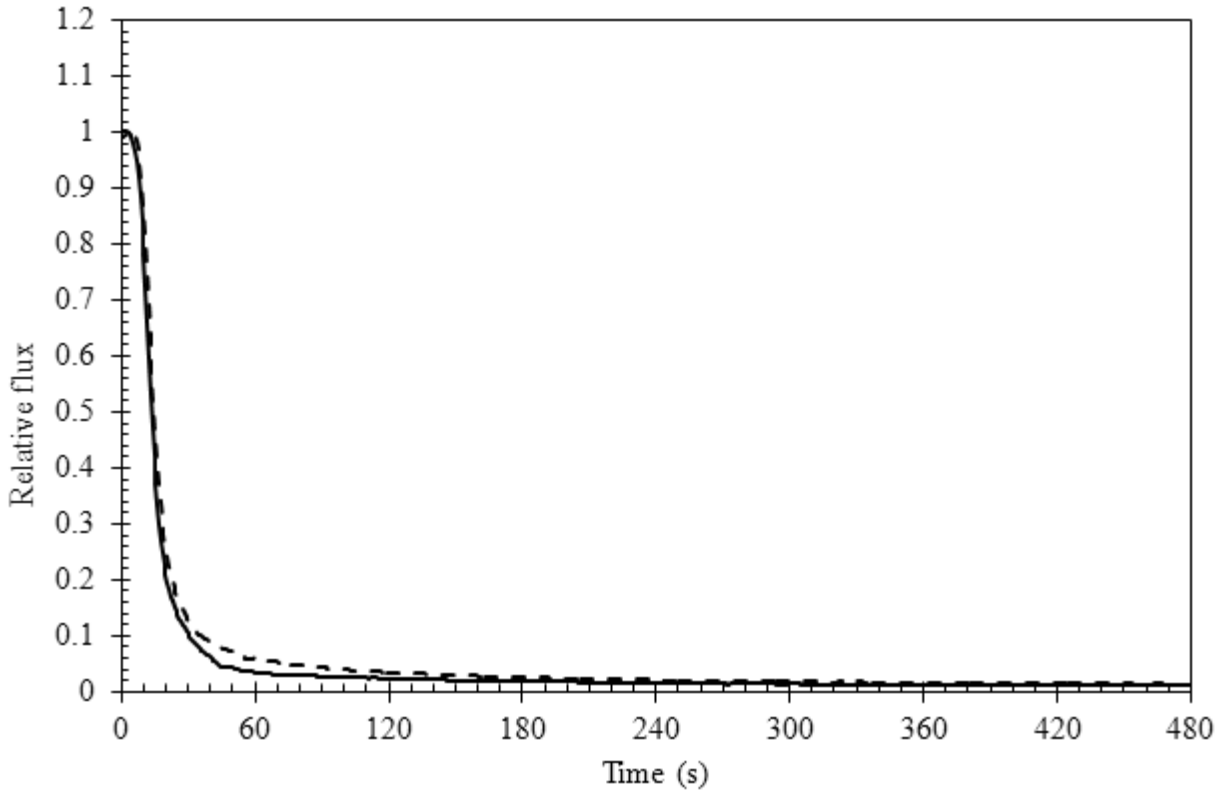

Figure 7. Typical flux decline curves produced during fouling of 5 μm microfiltration membranes with 0.09 vol% yeast suspension: TMP = 50 mbar, dashed line: TMP = 35 mbar. Re_{duct} = 1000 for both conditions. Initial fluxes were 20 000 and 15 000 $Lm^{-2}h^{-1}$ respectively.

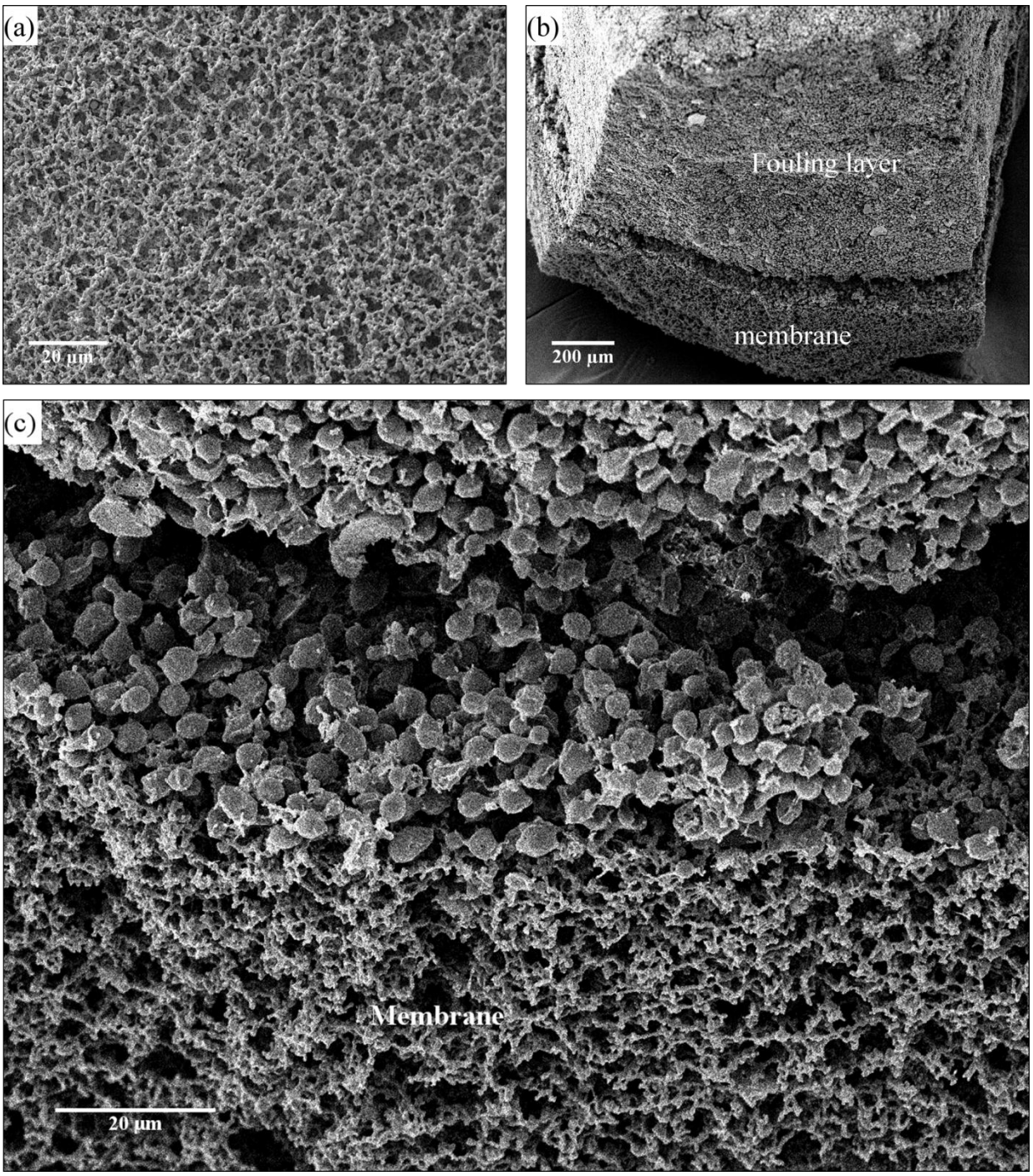

Figure 8. SEM images of: (a) virgin membrane at 1000× magnification, (b) fouled membrane at fractured edge under 200 × magnification, (c) fouled membrane at fractured edge under 1000× magnification. All images were recorded using 5 kV. Fouled membranes were produced by filtration of 0.09 vol% yeast suspension at TMP = 50 mbar and Re_{duct} = 1000 for 30 minutes.

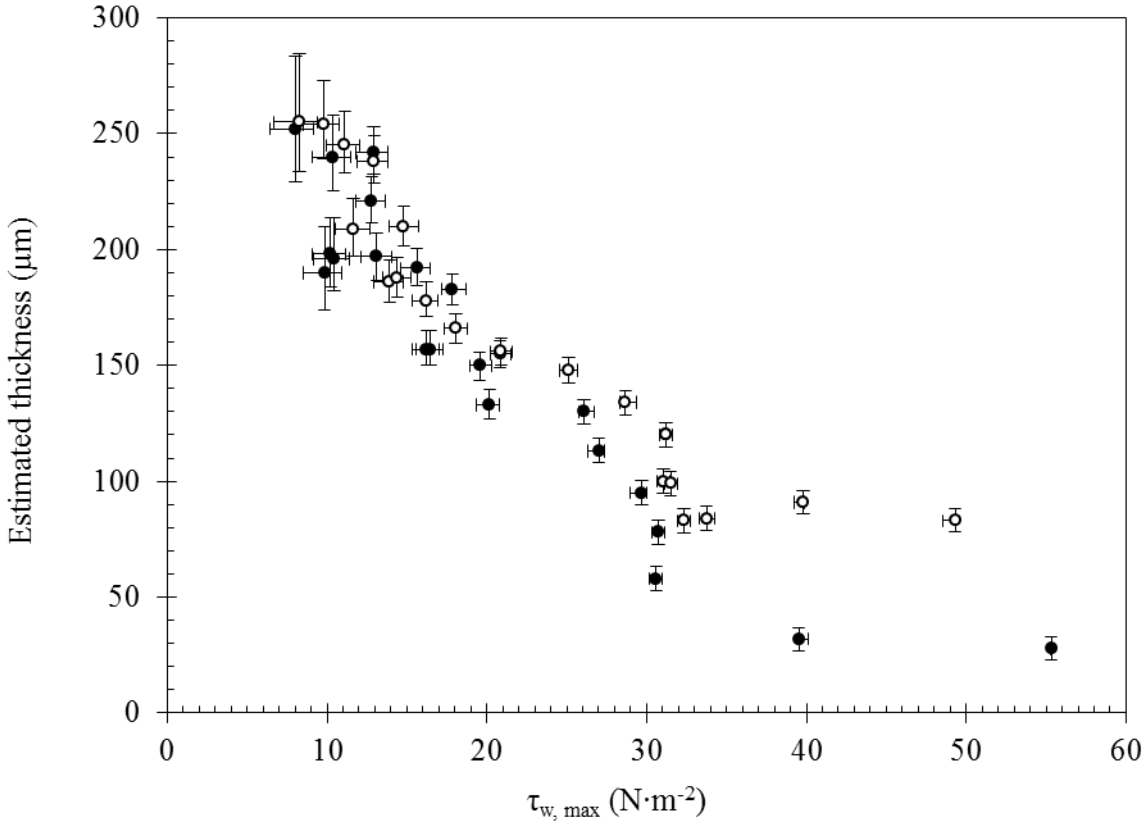

Figure 9. Estimated cake thickness against maximum imposed fluid shear for a cake formed with Re_{duct} = 1000. Closed symbols – TMP = 50 mbar, Open symbols – TMP = 35 mbar.

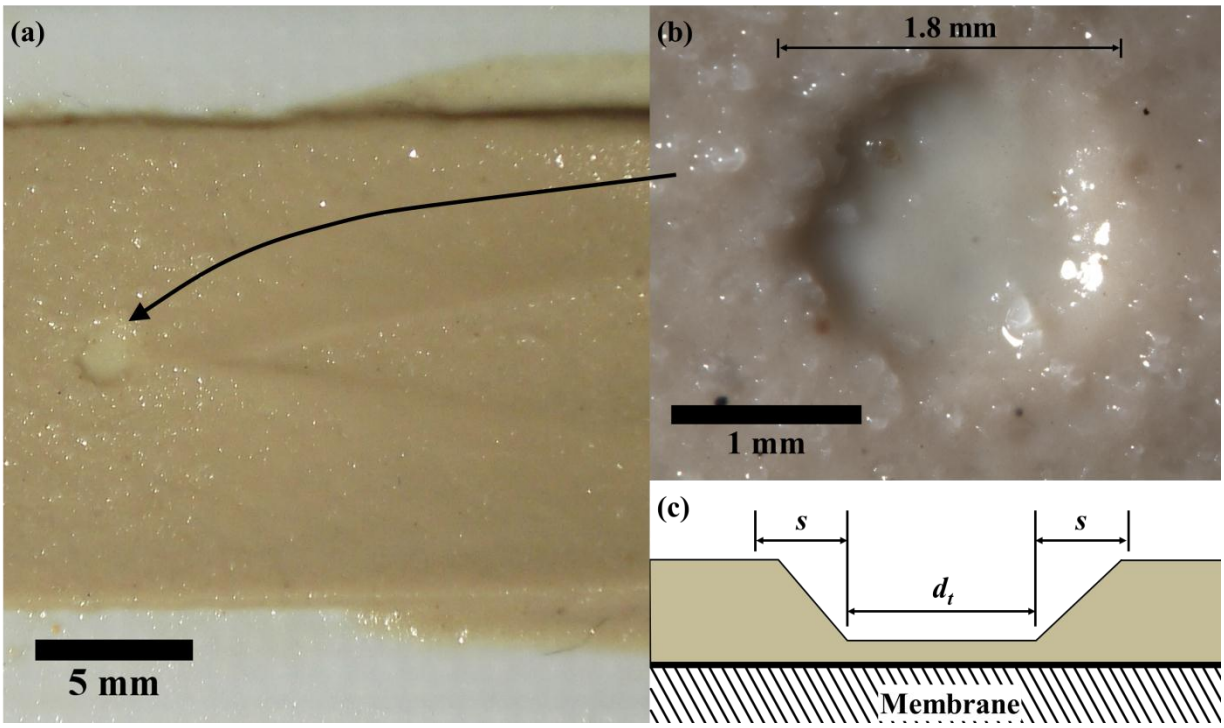

Figure 10. (a) and (b) Photographs showing the crater formed by deformation of the cake by FDG during analysis of preformed layers. The width of the eroded region (1.8 mm) falls between the diameter of the nozzle throat, d_t, and the outside edge of the nozzle rim, $d_t/2 + s$, as shown in (c), a representation of the cross section of the crater, in which the shape corresponds to the overhead view in (b). Direction of flow is from left to right.

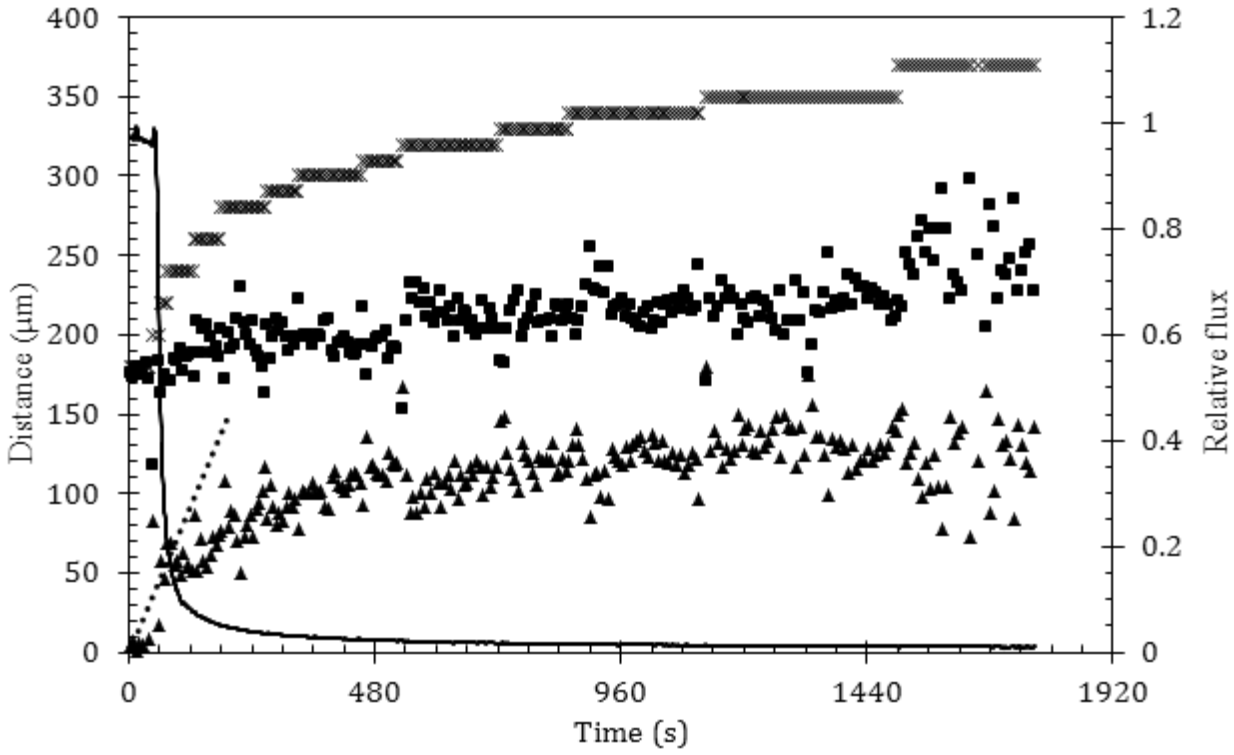

Figure 11. Thickness estimation and flux decline against time for a fouling run at TMP = 35 mbar and Re_{duct} = 1000. (×) h_0, (■) h, (▲) δ; the solid curve represents the relative flux (right axis) and the dotted line indicates the estimated initial growth rate of the cake.

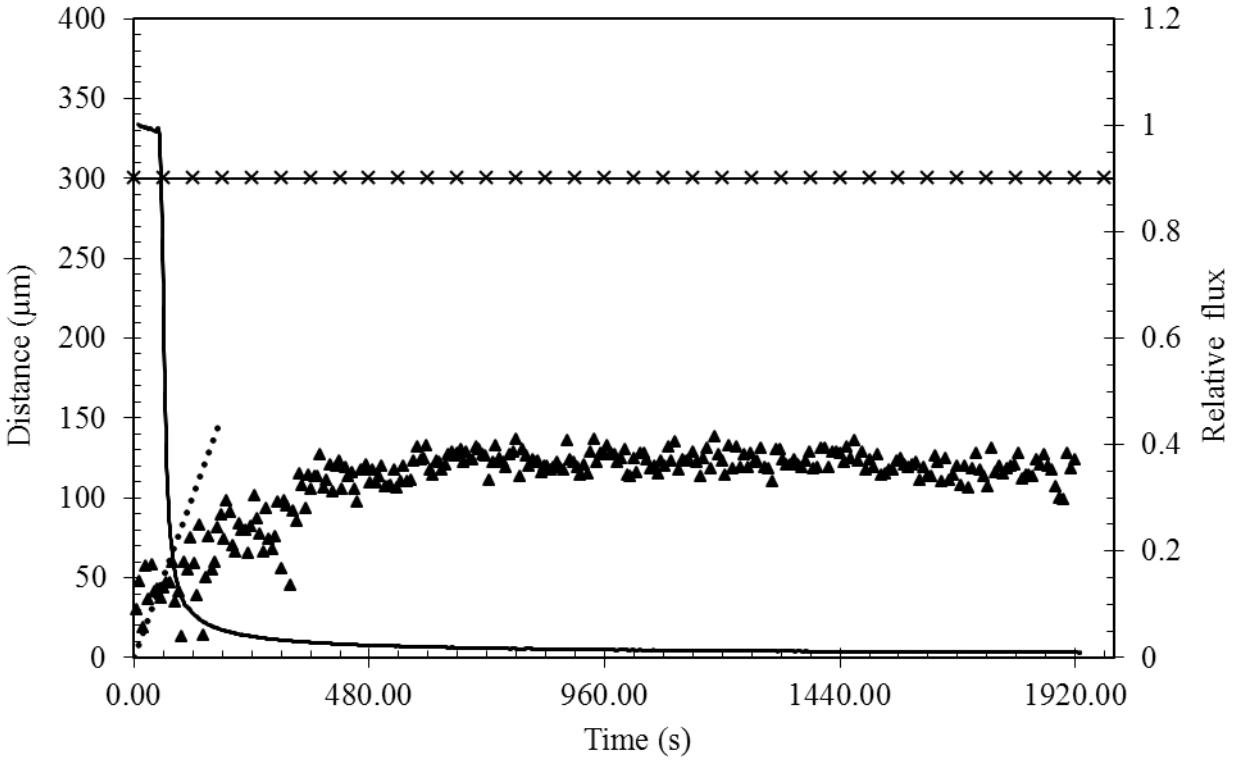

Figure 12. Estimated cake thickness against time at TMP =35 mbar, Re_{duct} = 1000, for static h_0 values of 300 μm. (▲) estimated thickness δ, (⁎) static gauge position, h_0. The solid line shows the relative flux (right axis), and the dotted line indicates the estimated initial growth rate of the cake.